Ionic Strength Dependent Transport of Microparticles in Saturated Porous Media: Modeling Mobilization and Immobilization Phenomena under Transient Chemical Conditions

TIZIANA TOSCO, ALBERTO TIRAFERRI, AND RAJANDREA SETHI*

DITAG - Dipartimento di Ingegneria del Territorio, Ambiente e Geotecnologie, Politecnico di Torino, Corso Duca degli Abruzzi 24, 10129 Turin, Italy

This study investigates ionic strength dependent deposition and release of microparticles in saturated porous media. Controlled micrometer-sized particle deposition experiments were conducted, followed by stepwise modifications in porewater chemistry to induce retained particle mobilization. A transient dual site transport model was tested against deposition and release, systematically addressing the effect of variations in solution ionic strength by coupling the equations for colloid transport with that for solute transport. The attachment and detachment coefficients of the model equations were explicitly tied to the salt concentration through proposed empirical functions, derived from experimental and theoretical considerations. Two regimes of attachment (and detachment) were hypothesized, showing favorable behavior beyond modeled values of a critical deposition concentration (and critical release concentration). Blocking phenomena were accounted for as well. This work shows how the intimate inclusion of salt concentration in a unique model equation system is able to describe *both* deposition and release behaviors of the particles under transient chemical conditions.

Introduction

Colloids, whether natural or anthropogenic, are extensively present in natural and engineered porous systems. Knowledge of the mechanisms controlling their mobility is required to understand their pathways and fate (*1*). On the one hand, some colloids represent a threat for humans or the environment because they are inherently hazardous or carriers of harmful contaminants sorbed on their surface (*2, 3*). On the other hand, many water treatment and remediation techniques rely on contaminant interaction with colloids, e.g. zero-valent iron nanoparticles (*4, 5*).

Traditionally, deposition of particles onto the solid matrix has been referred to as attachment and the opposite mechanism as detachment. Clean bed filtration theory (CFT) (*6*) can be certainly applied in favorable attachment conditions. However, many environmentally relevant particles such as microorganisms and clays and porous media are negatively charged at typical pH values, thus leading to unfavorable attachment conditions. Hydrodynamic and chemical factors strongly affect the mobility of colloids (*7–9*), and transport mechanisms also include blocking and ripening effects (*10, 11*) or deposition (release) in (from) the secondary energy minima (*9, 12*). Physical factors also play an important role, and some have been recently addressed more quantitatively by modeling processes such as straining and mechanical filtration (*13–16*).

Although retained colloidal particles in saturated porous media are generally immobile during constant-in-time geochemical and water flow conditions, mobilization is likely to occur under some circumstances. First, particle release may occur when the deposit on the media builds to the point that shear forces in the pore spaces resuspend more weakly retained particles (*17*). More often, retained particles can be released when changes in groundwater chemistry occur, thus increasing electrostatic repulsion interactions, e.g., lowering the solution ionic strength by recharge or freshwater intrusion. Previous studies have shown that solution chemistry is the principal factor affecting particle release (*17–22*). However, wide discrepancies in the extent, rate, and shape of release have been reported (*17–20, 22, 23*). A critical salt concentration for particle release has also been observed (*22, 24*). Systematic investigations and/or modeling in this direction have been presented by Grolimund et al. (*25*) and by Lenhart and Saiers (*22*). The authors have confirmed that mobilization is enhanced by lowering the ionic strength and have suggested the use of multiple components of particle population, distinguished on the basis of a threshold ionic strength of release (*22, 26*). Notwithstanding the ample literature on colloid transport, no systematic study has been presented proposing an all-inclusive unique transport model able to tie particle mobilization and immobilization to porewater solution chemistry.

Well-controlled microparticle transport column tests were performed in this study. After colloid injection in constant hydrochemical conditions, release of the retained particles was induced by step changes of porewater chemistry. On the basis of these tests, the present study develops a novel colloid transport model relative to saturated porous media, where *both* mobilization and immobilization onto the solid matrix are taken into consideration and the effect of changes in the solution ionic strength is systematically addressed and explicitly included into the model equations. The transient model is solved numerically with the implementation of a finite differences code and is proved accurate in reproducing experimental data. The partial differential equations for the salt and colloid concentrations are solved simultaneously, and explicit dependence of attachment and detachment coefficients on the ionic strength is expressed through empirical functions embedded in the model.

Theory and Mathematical Modeling

Coupled Dual Site Particle and Solute Transport Model. Colloid transport in saturated porous systems is usually described by a modified advection–dispersion equation, which includes an exchange term between the liquid and solid phases (*2*). In a 1D column apparatus

$$\begin{cases} n\dfrac{\partial c}{\partial t} + \rho_b\dfrac{\partial s}{\partial t} = nD\dfrac{\partial^2 c}{\partial x^2} - v\dfrac{\partial c}{\partial x} \\ \rho_b\dfrac{\partial s}{\partial t} = f(c, s) \end{cases} \qquad (1)$$

where c is the colloid concentration in the liquid phase [L^{-3}], s is the colloid concentration in the solid phase [M^{-1}], n is

* Corresponding author phone: +390115647735; fax: +390115647699; e-mail: rajandrea.sethi@polito.it.

the effective porosity of the porous matrix [-], ρ_b is the matrix bulk density [M L^{-3}], D is the colloid hydrodynamic dispersion coefficient [L^2 T^{-1}], ν is the darcyan velocity [L T^{-1}], and $f(c,s)$ is the generic nonequilibrium function that can describe chemically (attachment/detachment, blocking, and ripening), physically (mechanical filtration), and coupled physicochemically (straining) induced mass transfer between the liquid and solid phases (27). The high number of synergic phenomena and the system chemical variability lead to a complex description, while only in few particular cases one single process or interaction site can be considered dominant.

Chemical and physicochemical processes have been shown to be strictly dependent on ionic strength and pH (28). Therefore, colloid transport eqs 1 are to be coupled to those simulating the transport of different ions in solution. In this work, NaCl was used to modify ionic strength, and thus, a conservative tracer equation was added to the system (22). Two differently available interaction sites (both unfavorable to attachment) in the solid phase are hypothesized for the liquid−solid exchange term, following the heterogeneity of the sand materials outlined in the Experimental Section. Therefore, particle mobilization and immobilization are described by the transport model represented by the following set of partial differential equations

$$
\begin{cases}
n\dfrac{\partial c_t}{\partial t} = nD\dfrac{\partial^2 c_t}{\partial x^2} - \nu\dfrac{\partial c_t}{\partial x} \\[4pt]
n\dfrac{\partial c}{\partial t} + \rho_b\dfrac{\partial s_1}{\partial t} + \rho_b\dfrac{\partial s_2}{\partial t} = nD\dfrac{\partial^2 c}{\partial x^2} - \nu\dfrac{\partial c}{\partial x} \\[4pt]
\rho_b\dfrac{\partial s_1}{\partial t} = n\left(1 - \dfrac{s_1}{s_{\max,1}(c_t)}\right)k_{a,1}(c_t)c - \rho_b k_{d,1}(c_t)s_1 \\[4pt]
\rho_b\dfrac{\partial s_2}{\partial t} = nk_{a,2}(c_t)c - \rho_b k_{d,2}(c_t)s_2
\end{cases}
\tag{2}
$$

where c_t is the conservative salt concentration [M L^{-3}], s_1 is the particle concentration in solid phase [M^{-1}] for blocking sites S$_1$, $s_{\max,1}(c_t)$ is the maximum particle concentration for sites S$_1$, s_2 is the particle concentration in solid phase [M^{-1}] for sites S$_2$, $k_{a,i}(c_t)$ and $k_{d,i}(c_t)$ are the attachment and detachment coefficients for sites S$_i$. ν and D were assumed to be the same for particles and salt because the laboratory experiments did not show evidence of early colloid breakthrough due to size exclusion. The authors underline that the nature of the modeling procedure can be considered heuristic, whereby the different physicochemical phenomena are lumped together in transfer rate coefficients. The relationships of eqs 2 can be easily adjusted for each different system, also accounting for different particle populations in the interaction energies between deposited colloids (22). The model can also be targeted to reduce its overall degree of freedom. The relative importance of deposition and release from site S$_1$ compared to those of S$_2$ will be adjusted by imposing weights for the two site types, with the second site able to be switched off in case the porous medium is assumed homogeneous. The relationships describing the transfer of the two sites can also be adjusted to account for concurring attachment and detachment (for one site) and for straining mechanism (for the other site) (13).

Empirical Functions Express the Model Dependence on Solute Concentration. Salt concentration was included in the model through the following empirical relationships

$$
k_{a,i} = \frac{k_{a\infty,i}}{1 + \left(\dfrac{CDC_i}{c_t}\right)^{\beta_{a,i}}}
\tag{3}
$$

$$
k_{d,i} = \frac{k_{d0,i}}{1 + \left(\dfrac{c_t}{CRC_i}\right)^{\beta_{d,i}}}
\tag{4}
$$

$$
s_{\max,1} = \gamma_{s,1}c_t^{\beta_{s,1}}
\tag{5}
$$

where subscript i refers to sites S$_1$ and S$_2$, subscripts a refers to attachment and d to detachment. The terms $k_{a\infty,i}$, CDC$_i$, $\beta_{a,i}$, $k_{d0,i}$, CRC$_i$, $\beta_{d,i}$, $\gamma_{s,1}$, and $\beta_{s,1}$ are empirical coefficients determined via fitting procedures over the model eqs 2 for both sites, leading to a total number of 14 coefficients. These relationships were obtained through the analysis of the $k_{a,1}$, $k_{a,2}$, $k_{d,1}$, $k_{d,2}$, and $s_{\max,1}$ values found by interpolating the breakthrough curves. The relationship (3) for the attachment coefficients is modeled similarly to that of the CFT attachment coefficient α as a function of the prevailing electrolyte concentration (29). At ionic strength higher than a critical deposition concentration (CDC$_i$), repulsion forces tend to disappear, leading to a favorable (fast) attachment regime in which changes in salt concentration no longer affect the attachment coefficient ($k_{a\infty,i}$ represents the asymptotic value), while lower ionic strength leads to an unfavorable (slow) attachment regime (30). A conceptually similar behavior can be hypothesized for the detachment phenomenon in which the presence of a critical release concentration was experimentally observed here as well as in other studies mentioned above. Therefore, the relationship (4) hypothesizes that a critical release concentration CRC$_i$ defines the boundary between fast and slow detachment regimes. At low ionic strength, $k_{d,i}$ is limited at a maximum value $k_{d0,i}$ and not affected by c_t, and detachment can be considered favorable. For the maximum concentration on the solid phase in sites S$_1$, a power law was chosen in eq 5 consistent with previous results (11), which report a linear dependence of the logarithm of the maximum fractional collector surface coverage (directly related to $s_{\max}$) on the logarithm of the prevailing ionic strength.

Model eqs (2−5) were implemented in a Matlab environment using a finite differences scheme, thus allowing the calculation of ionic strength dependent attachment and detachment (Supporting Information). The software MNM1D can be downloaded from www.polito.it/groundwater/software.

Experimental Section

Materials. Monodisperse suspensions of 1.9 μm diameter latex microparticles with negatively charged carboxyl functional groups (Interfacial Dynamics Corporation, Portland, OR) were used as model colloids. Their stability, size, and monodispersity were confirmed using dynamic light scattering (Zetasizer Nano ZS90, Malvern Instruments Ltd., U.K.). Zeta potentials of the particles at pH 6.8 were found to range from −19.8 mV (at 25 °C and 600 mM monovalent cation) to −74.9 mV (at 25 °C and 1 mM monovalent cation). Values of −77 mV were measured in deionized water. Natural sand, mainly composed by quartz and with a minor content of K-feldspar, was employed (Sibelco Italia S.p.A., Robilante, CN, Italy), and thus, two different solid sites were implemented in the model. As illustrated below in Results and Discussion, our modeling site S$_1$ was found to behave in good accordance with a latex−quartz interaction, whereas site S$_2$ can be associated with a latex−feldspar system. The sand was cleaned and treated prior to use (5). The grains were sorted obtaining a diameter range of 150−300 μm and sonicated in a bath in 3 cycles of 10 min each to remove any detachable colloids. Column experiments were conducted over a range of ionic strengths by the addition of NaCl. Both eluant solutions and particle suspensions were buffered at pH 6.8 ± 0.2 by the addition of 0.1 mM NaHCO$_3$, unless otherwise stated.

Column System. The glass chromatography column with an inner diameter of 1.6 cm was wet packed with sand grains (35 g at dry conditions) to a mean height of 11.8 cm and vibrated to minimize layering or air entrapment. Column

characteristics were determined through fitting of conservative tracer breakthrough curves. Porosity was found to be equal to 0.42 ($\pm$0.02), and thus, the value of each pore volume PV equals 10.02 ($\pm$0.48) mL at a constant darcyan velocity of 7.91×10^{-5} ($\pm 1.67 \times 10^{-6}$) m/s.

Particle and tracer concentrations at the column inlet and outlet were monitored online using optical density measurements (at wavelengths of 750 and 190 nm, respectively) with a UV–vis spectrophotometer (Analytik Jena, Specord S600) and flow-through cells with optical lengths of 2 mm. Control particle-free experiments showed that a decrease in solution chemistry did not result in the release of colloidal material from the sand.

Procedure. The packed column was initially equilibrated by flushing with 2 PVs of deionized water and 10 PVs of the particle-free background electrolyte solution at the specific concentration employed for each deposition in order to eliminate traces of residual divalent cations (26). Experiments were then conducted in three phases: (i) Initially, particles suspended in the same initial solution chemistry (NaCl concentration of 1, 3, 10, 30, 100, and 300 mM for experiments A through F, respectively) were injected, part of which was deposited onto the sand surface. This was followed by pumping a particle-free background electrolyte solution. (ii) In the second phase, particle release was initiated by two-step reductions in ionic strength. Solutions were replaced by a particle-free electrolyte solution of reduced ionic strength and subsequently by deionized water. (iii) The last step of each experiment consisted of flushing a particle-free solution at a high pH of approximately 11 (achieved by addition of NaOH) to force the mobilization of all unreleased particles, thus evaluating the presence of irreversibly attached colloids. All experiments and related modeling were run in duplicate.

Results and Discussion

Particle Deposition and Release. Typical deposition and release curves are shown in the first column of Figure 1. The experimental data (gray $\bigcirc$) are displayed as normalized effluent particle concentration (c/c_0) as a function of time. The second column of Figure 1 presents the behavior after injection of a particle-free solution at high pH ($\sim$11), not included in the first plot.

(a) Particle Deposition. The breakthrough time for the particles at low salt concentration (deposition at 1, 3, and 10 mM in experiment A, B, and C, respectively) corresponds to 1 PV_t. Curves are steep, and the peak effluent concentration reaches the value of the influent concentration in a short time. Data are consistent with the estimation of the likely absence of energy minima for the lower ionic strengths for both sites (Supporting Information). Maximum particle concentration in the outlet is reached at later times in case of deposition at higher ionic strengths (30, 100, and 300 mM in experiment D, E, and F, respectively), suggesting enhanced removal of colloids and implying a higher surface coverage of sand. Estimated secondary energy minima are relatively deep in these cases, with absolute values larger than the thermal energy. In the case of ionic strength equal to 300 mM, no barrier to aggregation is anticipated, and particles will likely deposit in the primary minima for both sites.

(b) Mobilization of Deposited Particles. From the behavior of the profile following the lowering of ionic strength, one observes that little or no release peak occurred after the first step change. On the other hand, release peaks of increasing extent were observed after injection of DI at pH 6.8 (0.1 mM $NaHCO_3$) for test A–F. Higher release is shown for experiments E and F, consistent with a higher mass of colloids deposited in the solid phase. Comparison of the tracer and particle profiles suggests that the step change in solution chemistry immediately resulted in a pulse-

like release of particles. The release peak appeared within the end of the tracer front, suggesting the strong dependency of the release on the local salt concentration (31). The consequent colloid decline observed in the outlet exhibited a tailing behavior, consistent with previous observations (19, 31). Another important release peak was detected after the step change to the solution at pH 11. The registered peak was equal to or higher than the previous one for every set of experiments (Figure 1, second column).

As expected, values of the retained mass percentages registered in the experiments (Table S3 of the Supporting Information) increase for tests A– F. Before injection of the high pH particle-free solution, still a significant quantity of colloids was retained in the column. However, final mass balance values lie in the interval of $\pm$4%, suggesting that practically all of the injected colloids had initially deposited in the secondary energy minima and could be moved out of the packed bed after the final release step. This is obviously not true for experiment F only, whereby deposition in the primary minima makes particles not available for release.

(c) Particle Mobilization Behavior. Initial deposition of latex particles onto sand surfaces is not a readily reversible process. Mobilization of deposited particles is negligible when solution chemistry is not altered, and no observation of slow release occurs after the absorbance response returns to its baseline value (17). Because almost no particles were released after the first step change in solution chemistry, while high peaks are observed following injection of DI at pH 6.8, no correlation can be drawn between the release rate coefficients and the size of the energy minima (21). Here, as well as in previous studies (17, 19, 21), colloid release occurred suddenly when ionic strength reached a threshold beyond which colloids were mobilized. Ryan and Gschwend (1994) (21) found that this may occur at circumstances where the energy barrier to detachment disappears and repulsive forces exist at all separation distances. Attached colloids are then supposed to be "pushed" away from the surface. This finding suggests the existence of a critical release concentration (CRC) above which release is not favored and strongly limited, regardless of the chemistry at which the particles were initially deposited. CRC can be therefore related to a shift to a fast detachment regime occurring with the disappearance of the secondary minima. Nevertheless, in our system, even when the energy barrier to detachment virtually disappeared from the potential energy profiles, not all of the attached colloids were released from the surface. Recent studies (22) have underlined that the disappearance of an estimated energy barrier to detachment is not sufficient to cause complete release of retained particles. In fact, surface roughness and intragrain chemical variability cause the interaction energy between particles and mineral grains to be heterogeneous so that an even stronger "push" is actually needed to completely detach all particles obtained in our study by raising the pH to 11.

Model Application and Outcomes. The mathematical transport model fit was computed for each test, with the exception of the final release due to pH increase. Figure 1 presents profiles of simulated effluent particle (black line) and salt (gray line) concentration curves for the various experiments A–F. Regarding the deposition portion, the agreement between the fitted and experimental curves is fine in all cases. Also the fitting of the release part of the data is of good quality. The model described the little or no extent of colloid mobilization after the first step change in solution chemistry. Peaks following the injection of DI at pH 6.8 were correctly fitted as well; the computed line accurately follows the experimental data capturing timing, shape, and ad-
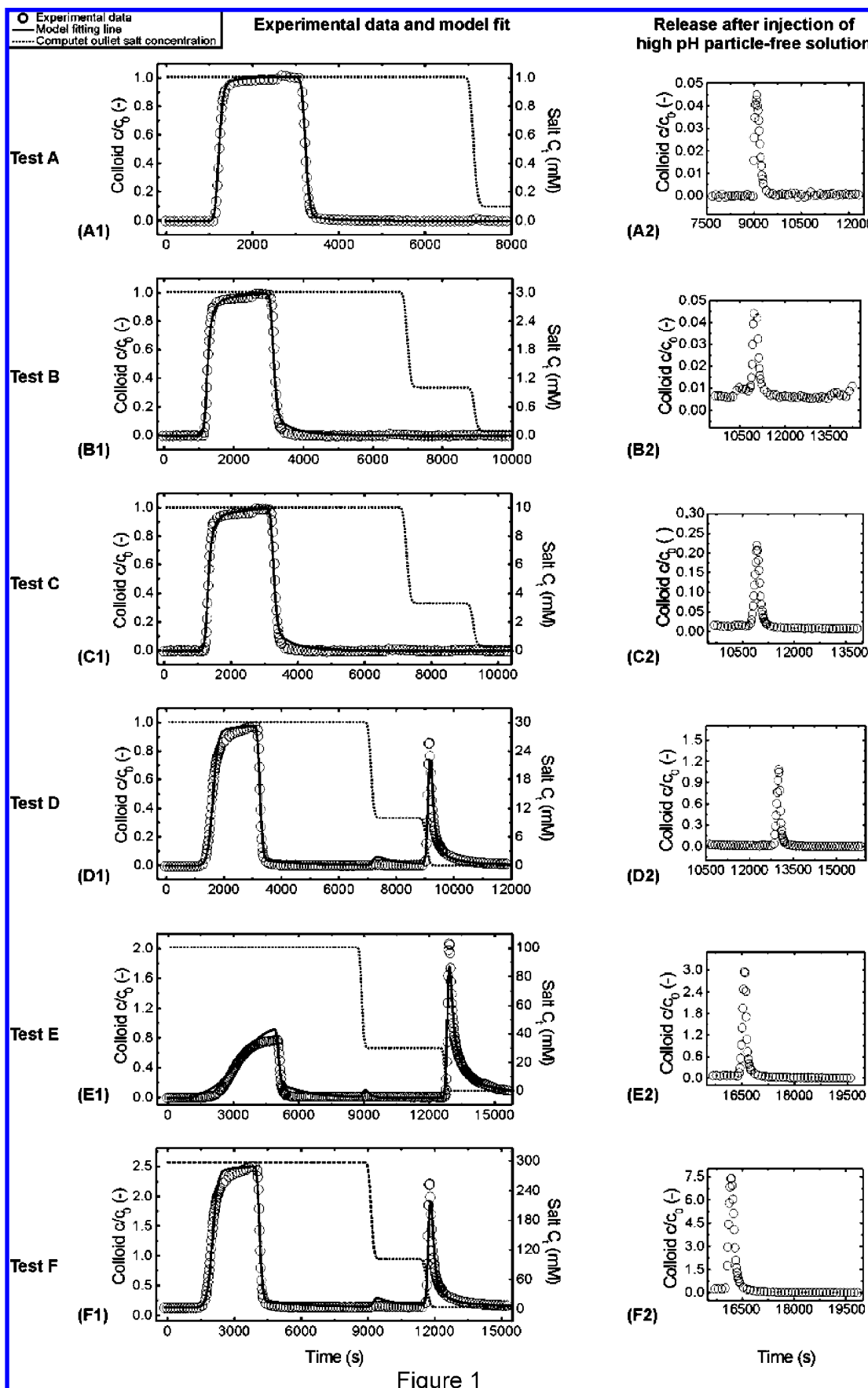
FIGURE 1. Observed and model-fitted effluent concentration curves for representative transport experiments. One breakthrough curve data set is plotted for each set of experiments. In the second column, profiles are plotted for registered particles in the outlet after injection of particle-free solutions at high pH. Please note the different scales on the *y* axis.
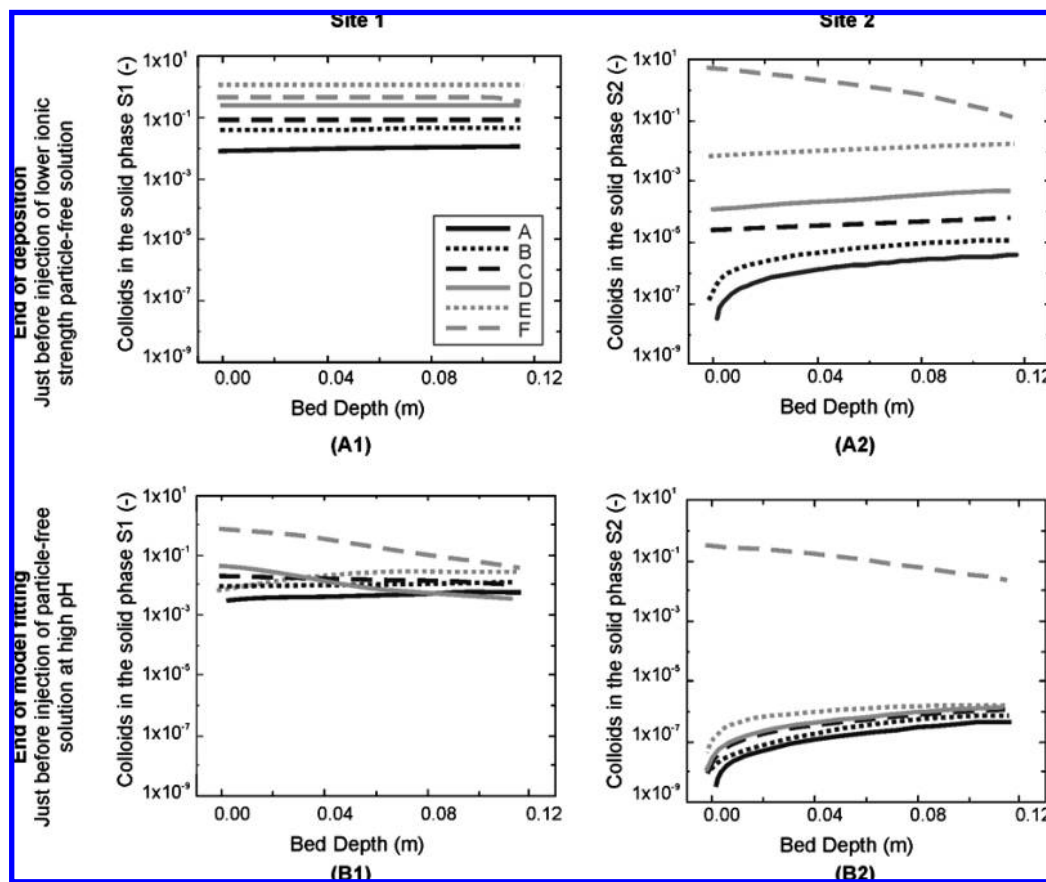
FIGURE 2. Modeled spatial distribution of retained particles at different times. Simulated data are plotted here as a dimensionless parameter $\rho_b s/c_0$ over the length of the packed bed. A1 and B1 show the distribution for the solid phase at site S1, A2 and B2 for the site S2. Plots A1 and A2 refer to the time at the end of the colloid deposition, just before the injection of a particle-free solution at lower ionic strength than that employed for the deposition. Plots B1 and B2 refer to the end time of the simulation, just before the injection of a particle-free solution at high pH.

equately depicting the magnitude of the release event, i.e., height of the peaks.

Figure 2 shows the simulated spatial particle distribution in the column at two different times and for the two different sites as a function of distance from the column inlet. The data are presented as dimensionless $\rho_b s_{fin}/c_0$, where s_{fin} is the final number of particles retained per dry mass of sand. Panels A1 and A2 of Figure 2 present the computed data at the end of the deposition part of the tests for interaction sites S_1 and S_2. Panels B1 and B2 of Figure 2 show results for the end time of the simulation. Deposition on site S_1 (Figure 2A1) was estimated to be relatively similar for all of the tests, with an almost constant fraction of mass retained along the column, i.e., the value of s_{max} was reached throughout the entire column at the end of the injection. This value increases for higher ionic strengths (*11*). Only at 300 mM NaCl, the saturation concentration is not reached everywhere. As for sites S_2 (Figure 2A2), the model describes quite different amounts of retained colloids for the different tests, with profiles not constant with *x*. A slight increase in retention was estimated along the bed depth for several ionic strengths as if the model depicted redeposition of released colloids in the second part of the column on this site type. The opposite behavior is observed for the deposition run at 300 mM, for which data are consistent with the release event trends and the overall mass balance.

At the end of the simulation run, profiles of colloids retained in sites S_1 for the different tests (Figure 2B1) are slightly lower than the corresponding ones of Figure 2A1. Profiles for the different tests are close together and still maintain a constant trend with *x*, with the exception of

experiment F. A greater variability was described for sites S_2 (Figure 2B2); profiles are largely lowered in Figure 2B2, reaching negligible values for almost all of the tests. This is not true for experiment F, where a significant mass of colloids was still estimated in the solid phase in panels A2 and B2 of Figure 2 for this test due to deposition in the primary minima as previously discussed.

Dependence of the Modeling Parameters on Ionic Strength. As described in Theory and Mathematical Modeling, for each test, the correlation between salt concentration and transfer rate was computed for the entire range of ionic strengths. Figure 3 shows simulated correlations of transfer rates and ionic strengths, and graphs are presented in log–log scale. As a consequence of the formulation of the empirical equations, values of $k_{a,1}$ and $k_{a,2}$ increase in Figure 3 as ionic strength increases, whereas the opposite trend is observed for the two detachment rate coefficients, $k_{d,1}$ and $k_{d,2}$.

The attachment coefficients have a linear dependence on ionic strength, with the estimated CDC_1 around 260 mM and CDC_2 higher than 400 mM, i.e., the attachment regime is unfavorable almost over the entire range of investigated ionic strengths (see Table S4 of the Supporting Information for numerical values of CDCs and other fitting coefficients). The model output regarding CDC values is reasonable, if compared to reported values in the literature for pure sodium systems (*4, 29*). In our case, one would expect CDCs to be fairly high, given the large values for outlet c/c_0, even at moderate ionic strengths, to be in the order of 300 mM for at least one site, and one would expect CDC_2 to be higher than CDC_1, given the larger repulsion estimated for the
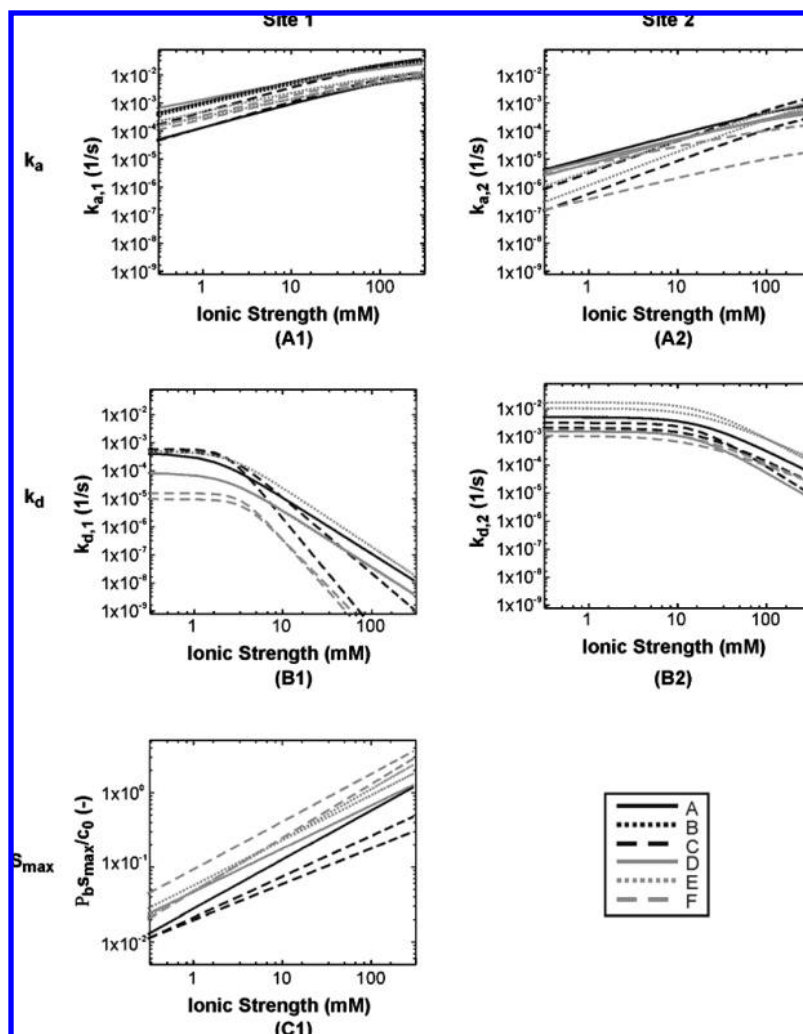
FIGURE 3. Modeled values of the colloid transfer rates from liquid to solid (A1, B1), from solid to liquid (A2,B2), and of the maximum concentration of colloids in the solid phase (C). Duplicates are included. Simulated data in panel C are plotted as dimensionless parameters $\rho_b s_{max}/c_0$, where s_{max} is the number of colloids normalized by the mass of dry sand at the end of the transport experiment.

latex−feldspar system (Supporting Information). This is consistent with the model outcome.

As opposed to the attachment coefficient, $k_{d,i}$ rates show a typical threshold behavior. CRC_1 is estimated to be 1−3 mM, and CRC_2 is found to be approximately 16 mM. It is not easy to compare these results with literature values as CRC was found to be dependent also on temperature (*24*) and fluid velocity (*17*). However, model outputs are here consistent with experimental observations; one would expect CRC_2 to be higher than CRC_1, with the latter on the order of a few millimolar, where we start observing significant release of deposited particles following the disappearance of the secondary minimum for site S_1. Furthermore, given the observed sudden release of retained particles beyond a threshold of solution chemistry, one would anticipate a sharp dependence of the detachment coefficient on the CRC/ionic strength ratio (*4*), i.e., relatively high values of exponent $\beta_{d,i}$. This is observed in our model outputs.

Consistent with the simulated values of Figure 2, $k_{a,1}$ tends to be higher than $k_{a,2}$. However, attachment associated with site S_1 tends to be less reversible in respect to changes in salt concentration, showing lower values than those related to S_2, i.e., values of $k_{d,1}$ are smaller than those of $k_{d,2}$. This is consistent with the latex−feldspar interaction

potential trends (site S_2), estimated to be on the whole more repulsive than those for the latex−quartz (site S_1) system.

Dimensionless values of $\rho_b s_{max}/c_0$ increase with ionic strength as expected from the blocking theory (*11, 32*). Overall, the profiles extrapolated from the different tests for each transfer rate and for s_{max} are close together.

Acknowledgments

Supporting Information Available

Numerical solution and function minimization, values of the retained mass percentages, quartz and feldspar energy profiles, schematic of the setup for transport experiments, numerical values of CDCs and other fitting coefficients, and parameter correlation matrix for the model fitted coefficients. This information is available free of charge via the Internet at http://pubs.acs.org.

Literature Cited

(1) Saiers, J. E.; Ryan, J. N. Introduction to special section on colloid transport in subsurface environments. *Water Resour. Res.* **2006**, *42* (12), W12S01, doi:10.1029/2006WR005620.

(2) Kretzschmar, R.; Borkovec, M.; Grolimund, D.; Elimelech, M. Mobile subsurface colloids and their role in contaminant transport. *Adv. Agron.* **1999**, *66*, 121–193.

(3) Kretzschmar, R.; Schafer, T. Metal retention and transport on colloidal particles in the environment. *Elements* **2005**, *1* (4), 205–210.

(4) Saleh, N.; Kim, H. J.; Phenrat, T.; Matyjaszewski, K.; Tilton, R. D.; Lowry, G. V. Ionic strength and composition affect the mobility of surface-modified Fe^0 nanoparticles in water-saturated sand columns. *Environ. Sci. Technol.* **2008**, *42* (9), 3349–3355.

(5) Tiraferri, A.; Sethi, R. Enhanced transport of zerovalent iron nanoparticles in saturated porous media by guar gum. *J. Nanopart. Res.* **2009**, *11* (3), 635–645.

(6) Yao, K.-M.; Habibian, M. T.; O'Melia, C. R. Water and waste water filtration: Concepts and applications. *Environ. Sci. Technol.* **1971**, *5*, 1105–1112.

(7) Bradford, S. A.; Yates, S. R.; Bettahar, M.; Simunek, J. Physical factors affecting the transport and fate of colloids in saturated porous media. *Water Resour. Res.* **2002**, *38* (12), 1327, doi: 10.1029/2002WR001340.

(8) Tufenkji, N.; Elimelech, M. Breakdown of colloid filtration theory: Role of the secondary energy minimum and surface charge heterogeneities. *Langmuir* **2005**, *21* (3), 841–852.

(9) Kuznar, Z. A.; Elimelech, M. Direct microscopic observation of particle deposition in porous media: Role of the secondary energy minimum. *Colloids Surf., A* **2007**, *294* (1–3), 156–162.

(10) Ryan, J.; Elimelech, M. Colloid mobilization and transport in groundwater. *Colloids Surf., A* **1996**, *107*, 1–56.

(11) Ko, C. H.; Elimelech, M. The "shadow effect" in colloid transport and deposition dynamics in granular porous media: Measurements and mechanisms. *Environ. Sci. Technol.* **2000**, *34* (17), 3681–3689.

(12) Torkzaban, S.; Tazehkand, S. S.; Walker, S. L.; Bradford, S. A. Transport and fate of bacteria in porous media: Coupled effects of chemical conditions and pore space geometry. *Water Resour. Res.* **2008**, *44* (4), W04403doi:10.1029/2007WR006541.

(13) Bradford, S. A.; Simunek, J.; Bettahar, M.; Van Genuchten, M. T.; Yates, S. R. Modeling colloid attachment, straining, and exclusion in saturated porous media. *Environ. Sci. Technol.* **2003**, *37* (10), 2242–2250.

(14) Bradford, S. A.; Bettahar, M. Straining, attachment, and detachment of Cryptosporidium oocysts in saturated porous media. *J. Environ. Qual.* **2005**, *34* (2), 469–478.

(15) Xu, S. P.; Gao, B.; Saiers, J. E. Straining of colloidal particles in saturated porous media. *Water Resour. Res.* **2006**, *42* (12), W12S16, doi:10.1029/2006WR004948.

(16) Bradford, S. A.; Simunek, J.; Bettahar, M.; van Genuchten, M. T.; Yates, S. R. Significance of straining in colloid deposition: Evidence and implications. *Water Resour. Res.* **2006**, *42* (12), W12S15, doi:10.1029/2005WR004791.

(17) McDowell-Boyer, L. M. Chemical mobilization of micron-sized particles in saturated porous media under steady flow conditions. *Environ. Sci. Technol.* **1992**, *26* (3), 586–593.

(18) Roy, S. B.; Dzombak, D. A. Colloid release and transport processes in natural and model porous media. *Colloids Surf., A* **1996**, *107*, 245–262.

(19) NocitoGobel, J.; Tobiason, J. E. Effects of ionic strength on colloid deposition and release. *Colloids Surf., A* **1996**, *107*, 223–231.

(20) Ryan, J. N.; Gschwend, P. M. Effect of solution chemistry on clay colloid release from an iron oxide-coated aquifer sand. *Environ. Sci. Technol.* **1994**, *28* (9), 1717–1726.

(21) Ryan, J. N.; Gschwend, P. M. Effects of ionic strength and flow rate on colloid detachment kinetics: Dependence on intersurface potential energy. *J. Colloid Interface Sci.* **1994**, *164*, 21–34.

(22) Lenhart, J. J.; Saiers, J. E. Colloid mobilization in water-saturated porous media under transient chemical conditions. *Environ. Sci. Technol.* **2003**, *37* (12), 2780–2787.

(23) Nelligan, J. D.; Kallay, N.; Matijevic, E. Particle adhesion and removal in model systems: V. Interpretation of the kinetics of particle detachment. *J. Colloid Interface Sci.* **1982**, *89* (1), 9–15.

(24) Khilar, K. C.; Fogler, H. S. The existence of a critical salt concentration for particle release. *J. Colloid Interface Sci.* **1984**, *101* (1), 214–224.

(25) Grolimund, D.; Borkovec, M. Release of colloidal particles in natural porous media by monovalent and divalent cations. *J. Contam. Hydrol.* **2006**, *87* (3–4), 155–175.

(26) Grolimund, D.; Borkovec, M. Long-term release kinetics of colloidal particles from natural porous media. *Environ. Sci. Technol.* **1999**, *33* (22), 4054–4060.

(27) Simunek, J.; He, C. M.; Pang, L. P.; Bradford, S. A. Colloid-facilitated solute transport in variably saturated porous media: Numerical model and experimental verification. *Vadose Zone J.* **2006**, *5* (3), 1035–1047.

(28) Ryan, J.; Elimelech, M. Colloid mobilization and transport in groundwater. *Colloids Surf., A* **1996**, *107*, 1–56.

(29) Grolimund, D.; Elimelech, M.; Borkovec, M. Aggregation and deposition kinetics of mobile colloidal particles in natural porous media. *Colloids Surf., A* **2001**, *191* (1–2), 179–188.

(30) Kretzschmar, R.; Borkovec, M.; Grolimund, D.; Elimelech, M. Mobile subsurface colloids and their role in contaminant transport. *Adv. Agron.* **1999**, *66*, 121–193.

(31) Grolimund, D.; Barmettler, K.; Borkovec, M. Release and transport of colloidal particles in natural porous media: 2. Experimental results and effects of ligands. *Water Resour. Res.* **2001**, *37* (3), 571–582.

(32) Kuhnen, F.; Barmettler, K.; Bhattacharjee, S.; Elimelech, M.; Kretzschmar, R. Transport of iron oxide colloids in packed quartz sand media: Monolayer and multilayer deposition. *J. Colloid Interface Sci.* **2000**, *231* (1), 32–41.